Journal of Structural Geology, Vol. 15, No. 7, pp. 911 to 922, 1993
Printed in Great Britain

0191-8141/93 $06.00+0.00

Progressive deformation of single layers under constantly oriented boundary stresses

RUUD WEIJERMARS*

Hans Ramberg Tectonic Laboratory, Institute of Earth Sciences, University of Uppsala, Box 555, S-751 22 Uppsala, Sweden

(*Received* 2 *December* 1991; *accepted in revised form* 31 *August* 1992)

Abstract—Competent single layers embedded in incompetent rock display a variety of structures if deformed by shortening or stretching: folds, boudins, or pinch-and-swells. Similarly, incompetent single layers hosted by more competent matrix rock may develop mullions, inverse folds, or both. The change in length of material planes with time is controlled by the type of bulk deformation and the initial layer orientation. The length and rotation history of material planes in a unit volume of rock is studied systematically by using, for the first time, deviatoric stresses of arbitrary—but constant—orientation making use of a fundamental deformation tensor. The traces of the eight planes in the unit volume of rock used in the analysis are in the plane of deformation and are treated as passive marker lines. The change in the length of these material lines is computed for arbitrary orientations of the principal deviatoric stresses. The history of the length change and rotation of the passive marker planes, carefully scaled against time, is subsequently used to predict the structures which would evolve in similarly oriented single layers of either competent or incompetent rock. The theoretical range of structural patterns evolving in the model is controlled by the orientations of the principal deviatoric stress. Conversely, the geometry of deformation patterns in nature can be used to constrain the possible orientations of the palaeostress axes.

INTRODUCTION

COMPETENT single layers embedded in incompetent rock may develop a variety of structures if deformed by shortening or stretching in the ductile field. Shortening instabilities are manifested as symmetric and asymmetric folds in the competent rock layer. Stretching instabilities occur as necks or pinch-and-swell structures which can separate into boudins. All these shear instabilities are caused by the resistance of competent layers to changes in their length whilst accommodating distortion due to shear stresses exerted at the interface with the incompetent matrix. The magnitude of these shear stresses is controlled by the deformation rate and the intrinsic viscosity contrast between the single layer and the matrix. The flow field in the vicinity of competent layers is complex and complete analytical solutions for the range of instabilities observed are not available (cf. Fletcher 1974, 1982, Smith 1975, 1977, 1979, Lloyd *et al*, 1982, Emermann & Turcotte 1984).

Ramsay (1967) has used a semi-analytical approach to predict from the change in length of material planes in a unit volume of rock whether shortening or stretching instabilities may develop (see also Becker 1893, Ramberg 1959, Flinn 1962, Ramsay & Huber 1983). This approach assumes that the nature and occurrence of the instabilities are controlled by the type of bulk deformation and the initial layer orientation. Ramsay (1967) considered only two cases of bulk, homogeneous deformation of the rock volume containing the competent rock layer: pure and simple shear. Both of these plane deformations imply a constant orientation for the principal stress axes with respect to a non-rotating boundary to the deforming volume, termed here the reference plane (Fig. 1). The principal deviatoric stress in pure shear is perpendicular to, and in simple shear at 45° to, the reference plane. Ramsay (1967) used these deformations in a graphical analysis to predict the orientations for which competent marker layers would buckle, unfold or stretch into boudins.

The present aim is to expand the systematic study of the length history of material planes in a unit volume of rock by using deviatoric stresses of arbitrary—but constant—orientation making use of a fundamental deformation tensor. The strategy followed here is as fol-

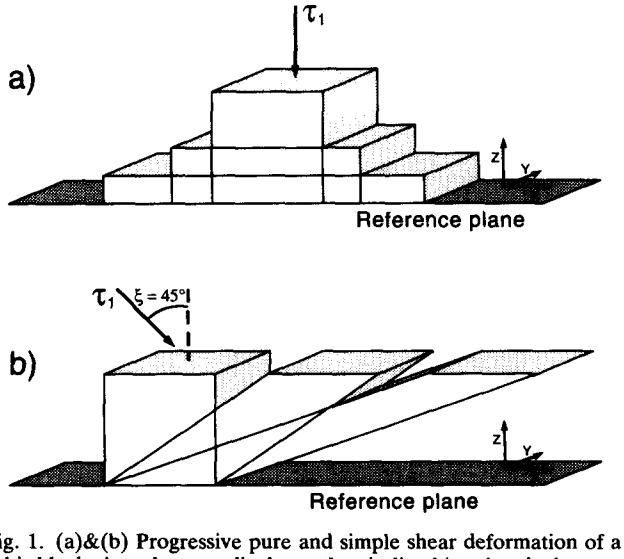

Fig. 1. (a)&(b) Progressive pure and simple shear deformation of a cubic block viewed perpendicular to the pin-line bisecting the bottom plane. Thus the block is in two equal parts, each slipping without friction over the reference plane in opposite directions. Increments of finite strain shown are 2 Ma apart for a rock of isotropic rheology deforming at a strain rate of $10^{-14}\,s^{-1}$.

*Present address: Department of Earth Sciences, King Fahd University of Petroleum and Minerals, 312 61 Dhahran, Saudia Arabia.

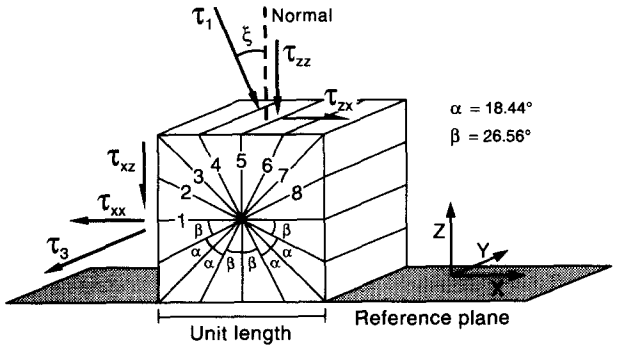

Fig. 2. Sketch section through the deforming unit volume to show the definitions of the angle, ξ, of the principal deviatoric stress, τ_1, with respect to the normal to the reference plane. Shown are the traces of eight differently oriented marker planes 1–8 for which the change in length and orientation are studied here.

lows. Figure 2 shows the traces of the eight planes in a unit volume of rock used in the analysis. These traces are in the plane of deformation and are treated as passive marker lines. The change in the length of these material lines is computed analytically for arbitrary orientations of the principal deviatoric stress. The history of the length change and rotation of the passive marker planes is subsequently used to predict the structures which would evolve in similarly oriented single layers, either more competent or less competent than the host rock. Figure 3(a) illustrates qualitatively the relation between the major principal stress axis and the orientation of folded and necked *competent* layers. Similarly, Fig. 3(b) illustrates qualitatively the angular relationship between the major principal stress axis and the orientation of mullions and inverse folds in *incompetent* layers (see next section).

The forward modelling of deformed competent layers in this analytical approach yields important implications for the interpretation of finite deformation patterns in nature. The orientation of the principal deviatoric stress and the associated orientation of the flow asymptotes

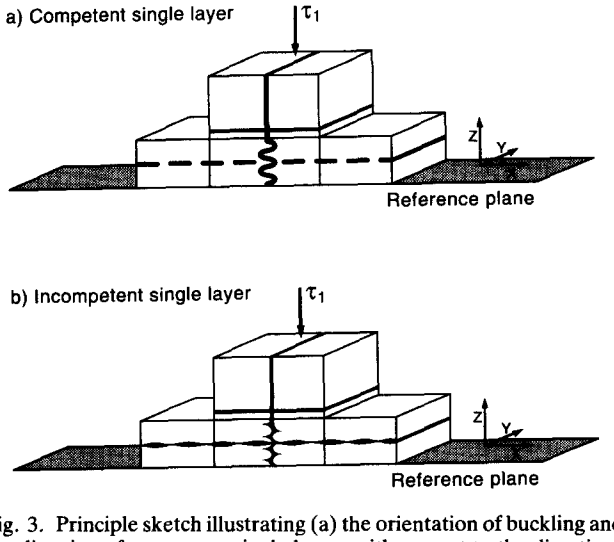

Fig. 3. Principle sketch illustrating (a) the orientation of buckling and boudinaging of competent single layers with respect to the directions of shortening and extension, and (b) the orientation of mullions and inverse folds of incompetent single layers with respect to the directions of shortening and extension.

controls the progressive deformation of material lines. The geometry of deformation patterns in nature can therefore be used to constrain the possible orientations of palaeostress axes in the limiting conditions assumed here. The term deformation is used here to include both the strain and rotation component of the distortion, but neglects any spin (rigid body rotation) or translation. This is achieved by choosing a reference frame fixed to the deformation structures inside the spinning and translating rock volume, so that estimates of palaeostress orientation are not affected by spin and translation.

PREVIOUS RESEARCH

Ramsay's (1967) graphical analyses of progressive deformation has been ground-breaking and maps the length history of material lines by superposition of finite and infinitesimal strain ellipses. The classical superposition method does not emphasize the position of the principal stress directions with respect to the rotating sectors separating lines of different stretching regimes. Figure 4 fixes the stress orientation for pure and simple shear deformations and summarizes the main features of the classical superposition method in a model which is, for the first time, geometrically scaled in all stages. The bulk deformation is assumed to be planar, isochoric and homogeneous. The assumption of homogeneous deformation means that all straight layers and material lines through the centre of the strain ellipse describe the deformation on the scale of that domain.

Figure 4(a) illustrates how the material lines initially occupy shortening and extending segments of Cauchy's infinitesimal strain ellipse. The fields of extension and shortening are separated by material lines that maintain their original length, equal to the diameter of the undeformed strain circle. Figure 4(b) shows how the material lines that at the onset of the deformation coincided with the non-material lines of no infinitesimal strain (A) will rotate to their new position (A*) after some finite strain. These particular material lines have never shortened and will asymptotically rotate towards the direction of maximum finite stretch which is rotating in non-coaxial deformations as indicated by the long axis of the finite strain ellipse. Figure 4(a) also outlines the material lines B* that will rotate to eventually coincide with the non-material lines of no finite strain (B) after some strain (Fig. 4b). Figure 4(c) superposes the shortening and extension fields of the infinitesimal and finite strain ellipses. This allows the distinction of four different segments in finite strain ellipses, each segment containing material lines with a characteristic length history.

Ramsay (1967) used the ellipses of superposed strain histories (Fig. 4c) to predict which markers will fold and which ones are likely to boudinage if more competent than the matrix rock. The caption of Fig. 4(c) explains that segments may contain material layers only shortened into folds (segment 1), only extended by necking into boudins or pinch-and-swells (segment 4), first shortened into folds that are being unfolded (seg-

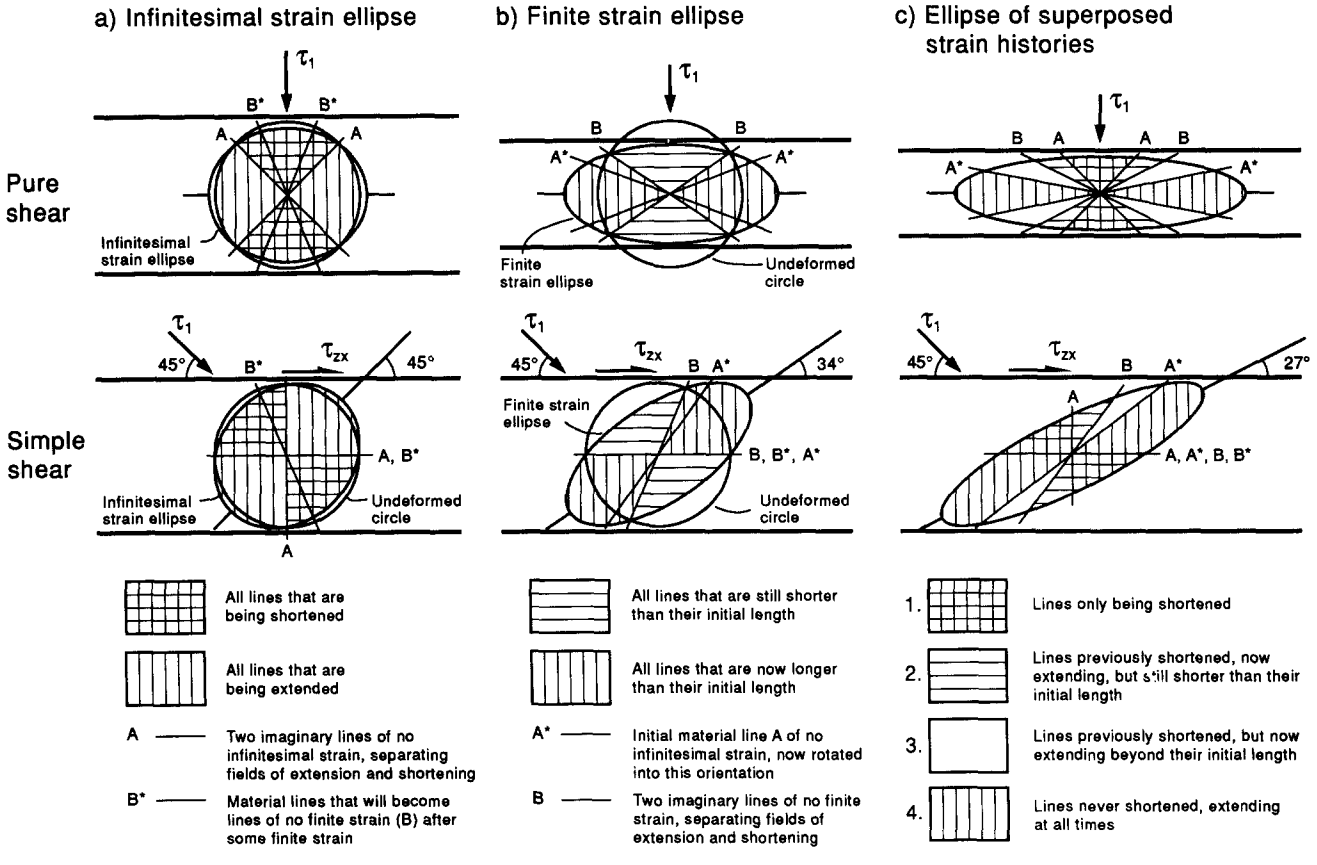

Fig. 4. Illustration of Cauchy's method of visualizing strain by ellipses of (a) infinitesimal or incremental strain, and (b) finite strain. Ramsay (1967) has extended this method in a systematic fashion by distinguishing four segments in what is here coined as (c) the ellipse of superposed strain histories. The four segments outlined for pure and simple shear are labelled 1–4. The length history of material lines is determined by the segments distinguished. It is possible to predict what structure would arise if the deformed rock segments were to contain competent or incompetent single layers. See text.

ment 2), or that have already been stretched beyond their initial length into boudins and pinch-and-swells (segment 3). This qualitative reasoning is supported by an extensive amount of analogue laboratory experiments on competent single layers visualizing the folding process for layer-parallel shortening (Ramberg 1959, 1967, 1981, Biot 1961, Ghosh 1966, Cobbold *et al.* 1971, Roberts & Strömgård 1972, Hudleston 1973, Johnson 1977, Abbassi & Mancktelow 1990), and boudinaging or pinch-and-swell formation for layer-parallel extension (Cloos 1947, Ramberg 1955, Paterson & Weiss 1968, Strömgård 1973, Gay & Jaeger 1975, Troëng 1975, Neurath & Smith 1982, Hildebrand-Mittlefehldt 1983, Bergman 1987). Similar dynamic conclusions may be drawn from numerical simulations of shortening of competent single layers into folds (Dieterich & Carter 1969, Shimamoto & Hara 1976, Anthony & Wickham 1978), and extension with necking into boudins (Selkman 1978, Lloyd & Ferguson 1981).

A minor novelty introduced here is the extension of Ramsay's (1967) arguments to predict what will happen to material lines if these are the contacts of incompetent single layers. Laboratory experiments have established that mullions or cuspate–lobate folds will form for layer-parallel shortening of incompetent single layers (Cobbold 1969, Sokoutis 1987, 1990). Layer-parallel extension of incompetent single layers produce theoretically predicted inverse folds (Smith 1975). Unpublished experiments at the University of Uppsala (Sokoutis personal communication) and field observations of incompetent basic dykes hosted in a gneissic basement (Talbot & Sokoutis 1992) suggest that inverse folds look similar to pinch-and-swells (Fig. 3b). It must be emphasized that inverse folds are rare and most incompetent layers are likely to extend uniformly. The four segments of Fig. 4(c), if containing incompetent single layers, will contain material lines only shortened into mullions (segments 1), only extended uniformly or rarely into inverse folds (segment 4), first shortened into mullions that may open by layer-parallel extension (segment 2), or that have already been stretched beyond their initial length into inverse folds (segment 3).

Other studies relevant to the present discussion are summarized here. Variations in the deformation patterns of cross-cutting veins of variable orientations before the onset of deformation have been used—applying the inverse of Ramsay's (1967) semi-analytical approach outlined above—to constrain the dimensions and orientation of the finite strain ellipsoid in suitable field exposures (Talbot 1970). Ramberg (1967) has demonstrated a tensor approach in which the orientation of strain markers that cut the ellipsoid of bulk or overall strain at different angles is used to determine the ellipsoid's axial ratio. Flinn (1962) summarized expressions which solve the inverse problem: the length of lines of arbitrary orientation within a strain ellipsoid follows

from the three angles with the principal strain axes. None of these expressions allow quantitatively following the history of changes in length and orientation of material lines, because the displacement gradient tensor was not formulated in time-dependent terms.

Passchier (1986, 1990a,b) focused on establishing the orientation of the incremental stretching axes by relating shear zone patterns to the kinematic vorticity number. However, practical application of this approach is limited because the orientation of Passchier's (1986, 1990a,b) flow patterns *is not appropriately related to physical boundaries of the deformation zone* (compare with flow patterns in Weijermars 1991). Passchier *et al.* (1990) and Hanmer & Passchier (1991) emphasized that all material lines will rotate towards the maximum instantaneous stretching axis. It is shown here how these stretching axes relate to the physical boundaries of a deformation zone, and how stretching axes rotate towards the asymptotes of the flow field. The present study further emphasizes the significance of the relative orientation of the bulk axes of principal stress and finite stretching. The tensor approach allows inclusion of the time scale of the deformation, in both dimensional and non-dimensional form.

METHOD

An arbitrary deformation is fully described by the following point transformation:

$$(x,y,z) = \mathbf{F}(x_0,y_0,z_0), \tag{1}$$

where (x_0,y_0,z_0) and (x,y,z) are the position vectors of an arbitrary material particle before and during deformation and **F** is the deformation tensor. Solutions of the components of the tensor **F** can be obtained by integrating the rate of displacement or velocity gradient equations over time.

Ramberg (1975a,b) first used equations for particle movement paths in a study of progressive deformation involving superposition of simple and pure shear deformations. Weijermars (1991) simplified the analytical description of progressive deformation by deriving a tensor for deformation caused by a deviatoric stress of a constant orientation. This deformation tensor was used to forward model the progressive deformation of a unit volume of rock in response to deviatoric stresses of various constant orientations (Weijermars 1991). The same approach is used here to visualize the length history of material lines.

In the case of homogeneous plane strain in the XZ-plane, with the X-axis chosen parallel to a non-rotating, free-slip boundary to the deforming volume (Fig. 5a) only four of the nine components of the deformation tensor are non-zero. This detachment boundary may be interpreted as a stretching fault, using a new terminology for faults active contemporaneous with ductile deformation of the wall rock (Means 1989, 1990). The detachment may accommodate either shortening or extension stretch, and may be rotating or

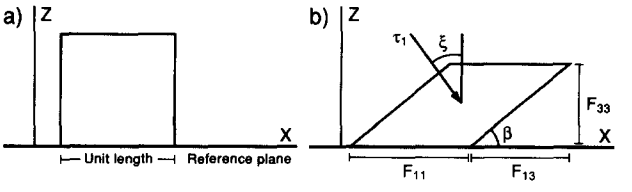

Fig. 5. (a)&(b) Principle sketches through the deforming unit volume to show the definitions of the constant angle, ξ, of the arbitrary principal deviatoric stress, τ_1, with respect to the normal to the reference plane. The deformation tensor components F_{11}, F_{13} and F_{33} relate to physical dimensions as indicated. See text.

spinning. For practical reasons, the spin is neglected and the reference frame is kept fixed to the detachment plane at all times. The four non-zero tensor components are (Weijermars 1991):

$$F_{11} = \exp(R_t \cos 2\xi) \tag{2a}$$

$$F_{22} = 1 \tag{2b}$$

$$F_{33} = F_{11}^{-1} \tag{2c}$$

$$F_{13} = (F_{11} - F_{11}^{-1}) \tan 2\xi, \tag{2d}$$

where the only two independent variables are ξ, the angle between the largest principal deviatoric stress, τ_1, and the normal to the reference plane (Fig. 5b), and the non-dimensional time $R_t = t\dot{e}_1$. Arbitrary quantities are time t and principal strain rate $\dot{e}_1$. Positive angles of ξ are measured anti-clockwise from the normal to the reference plane. The tensor component $F_{22} = 1$ accounts for the plane isochoric deformation so that $y = y_0$ at all times.

Figures 5(a) & (b) explain how the tensor components F_{11}, F_{13} and F_{33} are physically measurable as the normalized dimensions of a model cube deforming along a detachment horizon. F_{11}, F_{13} and F_{33} can be used to express the change in length, $L(R_t)$, of any marker in terms of ξ and R_t. Figures 6(a)–(h) illustrate how F_{11}, F_{13} and F_{33} determine the lengths of lines 1–8, normalized by the initial length unit of F_{11}. The corresponding analytical expressions are:

$$\text{Line 1: } L_1(R_t) = F_{11} \tag{3a}$$

$$\text{Line 2: } L_2(R_t) = [[F_{11} - (F_{13}/2)]^2 + (F_{33}/2)^2]^{1/2} \tag{3b}$$

$$\text{Line 3: } L_3(R_t) = [(F_{11} - F_{13})^2 + F_{33}^2]^{1/2} \tag{3c}$$

$$\text{Line 4: } L_4(R_t) = [[(F_{11}/2) - F_{13}]^2 + F_{33}^2]^{1/2} \tag{3d}$$

$$\text{Line 5: } L_5(R_t) = (F_{13}^2 + F_{33}^2)^{1/2} \tag{3e}$$

$$\text{Line 6: } L_6(R_t) = [[(F_{11}/2) + F_{13}]^2 + F_{33}^2]^{1/2} \tag{3f}$$

$$\text{Line 7: } L_7(R_t) = [(F_{11} + F_{13})^2 + F_{33}^2]^{1/2} \tag{3g}$$

$$\text{Line 8: } L_8(R_t) = [[F_{11} + (F_{13}/2)]^2 + (F_{33}/2)^2]^{1/2}. \tag{3h}$$

Substitution of expressions (2a), (2c) and (2d) into (3a)–(3h) eliminates tensor components F_{11}, F_{13} and F_{33} and yields line lengths as functions of ξ and R_t. The change in inclination of the marker line with respect to the X-axis, ϕ, measured clockwise as indicated in Fig. 6, is:

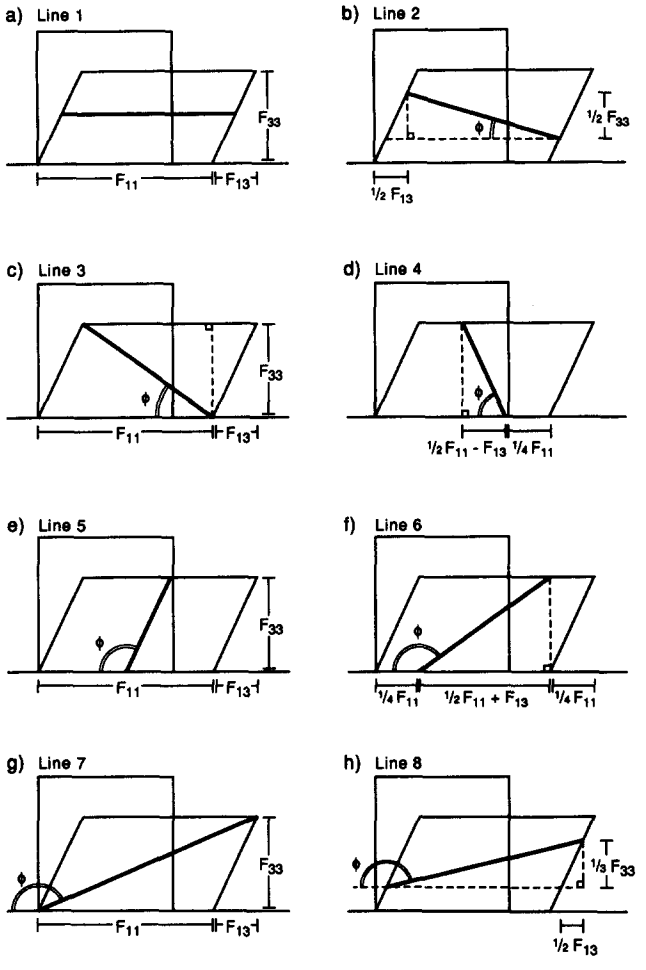

Fig. 6. (a)–(h) The length of passive line markers 1–8 can be expressed in terms of tensor components F_{11}, F_{13} and F_{33}, using the Pythagoras formula (equations 3a–3h). The orientation, ϕ, of the marker lines with respect to the horizontal X-axis may also be expressed in terms of tensor components F_{11}, F_{13} and F_{33}, using simple goniometric formulas (equations 4a–4h).

$$\text{Line 1: } \phi_1(R_t) = 0° \tag{4a}$$

$$\text{Line 2: } \phi_2(R_t) = \tan^{-1}[F_{33}/(2F_{11} - F_{13})] \tag{4b}$$

$$\text{Line 3: } \phi_3(R_t) = \tan^{-1}[F_{33}/(F_{11} - F_{13})] \tag{4c}$$

$$\text{Line 4: } \phi_4(R_t) = \tan^{-1}[F_{33}/[(F_{11}/2) - F_{13}]] \tag{4d}$$

$$\text{Line 5: } \phi_5(R_t) = 180° - \tan^{-1}(F_{33}/F_{13}) \tag{4e}$$

$$\text{Line 6: } \phi_6(R_t) = 180° - \tan^{-1}[F_{33}/[(F_{11}/2) + F_{13}]] \tag{4f}$$

$$\text{Line 7: } \phi_7(R_t) = 180° - \tan^{-1}[F_{33}/F_{11} + F_{13})] \tag{4g}$$

$$\text{Line 8: } \phi_8(R_t) = 180° - \tan^{-1}[F_{33}/(2F_{11} + F_{13})]. \tag{4h}$$

Lines 2, 3 and 4 will rotate through the vertical given sufficient time. If this happens, ϕ will be smaller than 0° in the analytical expressions (4b)–(4d). It is therefore necessary to append an IF statement to expressions (4b)–(4d) saying that, for $\phi < 0°$, $\phi = 180° + \phi$.

RESULTS

Equations (3a)–(3h) and (4a)–(4h) have been evaluated and summarized in a series of graphs. The time steps used in the computations are scaled by absolute times, t, according to:

$$t = R_t/\dot{e}_1. \tag{5}$$

Scaling of absolute times is possible after adopting a characteristic geological strain rate of 10^{-14} s^{-1}, and non-dimensional R_t units of 0.315 for each Ma. Figures 7 and 8 represent a selection of the generated graphs using material lines 1, 3, 5, 6 and 7. Figure 7 illustrates the change in length of these lines with time; Fig. 8 plots their corresponding change in orientation with time using expressions (4a)–(4h).

Figure 7 plots the change in length of single lines for pure shear ($\xi = 0°$ and $\xi = 90°$), simple shear ($\xi = 45°$) and intermediate stress orientations $\xi = 10°$, 20°, 30°, 40°, 50°, 60° and 70°. Of all eight lines evaluated, line 1 (parallel to the detachment) provides the largest range in stretches for $0° \leq \xi \leq 90°$, lying in both the extensional and shortening field. In contrast, line 7 will never show any shortening and will extend in a fashion which—for the first 5 Ma—is practically insensitive to variations in the principal stress orientation. In general, all material lines rotate away from the major principal stress axis and therefore will eventually stretch. Exceptions are lines parallel to the X-axis (line 1), which do not rotate, but shorten for $45° < \xi \leq 90°$, extend for $0° \leq \xi < 45°$, and maintain constant length for simple shear, i.e. $\xi = 45°$.

Figure 7 further shows that, in pure shear deformations ($\xi = 0°$ and $\xi = 90°$), all lines will extend continuously except for lines parallel to the principal stress axes. For simple shear deformations ($\xi = 45°$), all lines will have stretches larger than unity after about 7 Ma. The length of lines parallel to the stretching fault remains unchanged. For $0° < \xi < 45°$, some lines suffer initial shortening, but these will extend later so that eventually no line remains shorter than its initial length given sufficient time. For $45° < \xi < 90°$, there is very little initial shortening of any material lines. All lines will have stretches larger than unity after about 10 Ma, except for lines parallel to the stretching fault.

Figure 8 emphasizes that line 1, parallel to the detachment, may shorten or extend but will not rotate at all. It also shows that line 5 will always rotate in the same, clockwise direction as ϕ consistently increases for any ξ and never decreases. The remaining material lines may either rotate clockwise or anti-clockwise, depending upon the orientation of the principal stress. All rotating material lines will tend to align after about 8 Ma of deformation. This is exactly true for all lines deforming by principal deviatoric stress orientations $0° < \xi \leq 45°$, as these lines can be seen to rotate towards parallelism with the X-axis. For pure shear deformation ($\xi = 0°$ and $\xi = 90°$), all lines will still rotate towards parallelism with the X-axis, but lines which are parallel to the major ($\xi = 0°$) and minor ($\xi = 90°$) principal stress axes stay perpendicular to the X-axis. For deformations where $45° < \xi < 90°$ all lines except for line 1 rotate towards a direction of maximum stretch which is not parallel to the X-axis but aligned with the orientation of the extensional flow asymptote (see later).

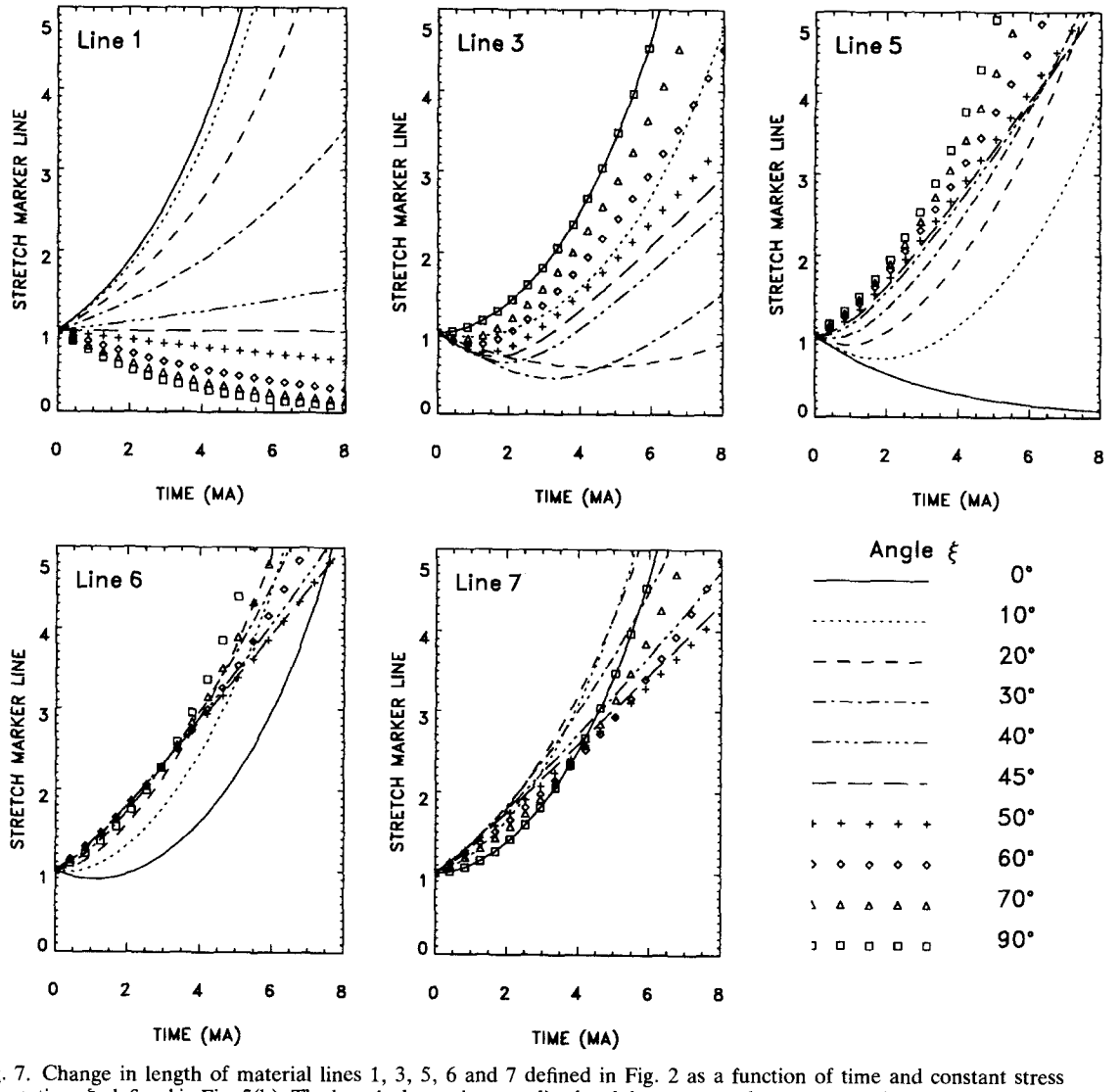

Fig. 7. Change in length of material lines 1, 3, 5, 6 and 7 defined in Fig. 2 as a function of time and constant stress orientation, ξ, defined in Fig. 5(b). The length change is normalized and thus expressed as a stretch. The time scale is valid for a principal geological strain rate of 0.315 Ma^{-1} or 10^{-14} s^{-1}. Governing expressions are equations (3a)–(3h). All lengths are normalized by their own initial length according to $L^* = L(R_t)/L(0)$.

GENERALIZATION

Figures 9(a)–(e) show the progressive deformation of a unit cube at 2 Ma intervals for a strain rate of 10^{-14} s^{-1} for $\xi = 0°$, 30°, 45°, 60° and 80°. The bulk deformation remains homogeneous because there is free slip at the base of the deforming unit volume. Strain gradients in the direction perpendicular to natural stretching faults may still be accounted for by choosing subdomains small enough to approximate homogeneous deformation. The graphs of Figs. 7 and 8 were used to reconstruct the stretching and rotation history of each of the eight marker lines used in Fig. 9. The structures indicated assume a competent single layer. A similar diagram could be constructed for incompetent single layers, but is considered redundant.

Figure 8 illustrated how all material lines will tend to rotate away from the principal stress axis and become subparallel to the direction of maximum stretch. The direction of maximum finite stretch is indicated in Fig. 9 by the extensional flow asymptote. The material lines are subparallel to the extensional flow asymptote after about 8 Ma of deformation, except for those coinciding with the direction of the compressional flow asymptote. For principal deviatoric stress orientations $0° \leq \xi \leq 45°$, the direction of maximum stretch is parallel to the stretching fault or the X-direction. For deformations where $45° < \xi \leq 90°$ the direction of maximum stretch is not parallel to the X-axis but aligned with the orientation of the extensional flow asymptote. Rotation of material lines towards parallelism with the extensional flow asymptote occurs faster in pure shear than in less efficient simple shear deformation.

The range of maximum finite stretch in Fig. 9 ranges between 3 and 3.5 after 4 Ma of deformation at 10^{-14} s^{-1} depending upon stress orientation. Strain analyses of naturally deformed rocks indeed suggest that most deformation patterns take about 1–5 Ma to develop, whereas stretches range mainly between 1 and 3 (Pfiffner & Ramsay 1982). Figure 9 illustrates that the occurrence of folds would become progressively unlikely if finite strains increase. The amount of rotation of

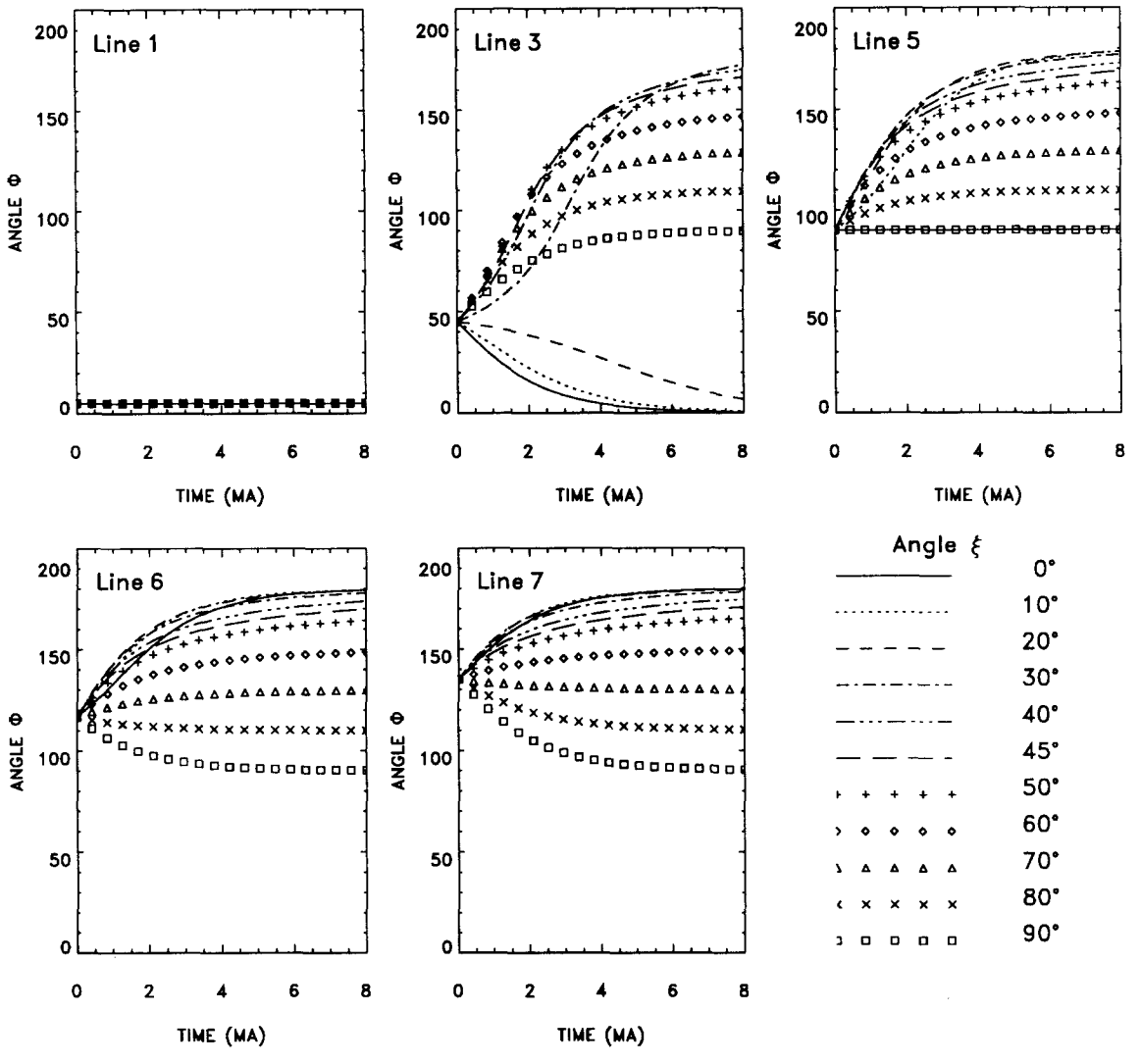

Fig. 8. Change in orientation of material lines 1, 3, 5, 6 and 7 defined in Fig. 2 as a function of time and constant stress orientation, ξ, defined in Fig. 5(b). The orientation, ϕ, is measured as indicated in Figs. 6(a)–(h). The time scale is valid for a principal geological strain rate of 0.315 Ma^{-1} or 10^{-14} s^{-1}. Governing expressions are equations (4a)–(4h).

the boudins and minor folds in Fig. 9 is arbitrary, but the sense of rotation is in accordance with experiments and theory of Ghosh (1966) and Ghosh & Ramberg (1966). Although the theory developed here describes the stretch and rotation of passive markers, this will closely approximate the deformation history of the enveloping surface of active marker layers. This is because the bulk strain rate is unlikely to be affected by the rheology of the single layer as it occupies, in this model approach, only a minor portion of the total volume involved in the deformation. Likewise, the vorticity of the active layer is constrained by the two half spaces of rock at either side of the single layer, as transport of the host rock across the single layer is negligible.

The orientation of the direction of maximum finite elongation in Fig. 9, indicated by the extensional flow asymptotes, is controlled by the stress orientation. It may therefore be interesting to elaborate the angular relationship between the major deviatoric stress axis and the extensional flow asymptote, as these are not necessarily perpendicular. The flowlines of plane deformation can be most concisely represented by the following stream function (Weijermars & Poliakov in press):

$$\psi = \dot{e}_1 (xz \cos 2\xi + z^2 \sin 2\xi). \quad (6)$$

It follows from expression (6) that the stream function ψ is fully described if the orientation ξ of the principal deviatoric stress is known together with the principal strain rate $\dot{e}_1$. The flow pattern and associated fluid deformation are fixed by ξ whilst $\dot{e}_1$ is nothing but a scaling parameter only controlling the rate of flow, not affecting the deformation path. Expression (6) is only valid for the particular orientation of the co-ordinate axes shown in Fig. 5. A stream function for the same deformation, but with a reference frame always oriented at 45° to the principal deviatoric stress axis, has been discussed elsewhere (Weijermars 1991, equation 3).

Figure 10(a)–(e) shows the full flow patterns governing the corresponding deformations shown in Figs. 9(a)–(e), using $\xi = 0°, 30°, 45°, 60°$ and 80° and arbitrary strain rate $\dot{e}_1$. The hyperbolic streamline patterns all possess a

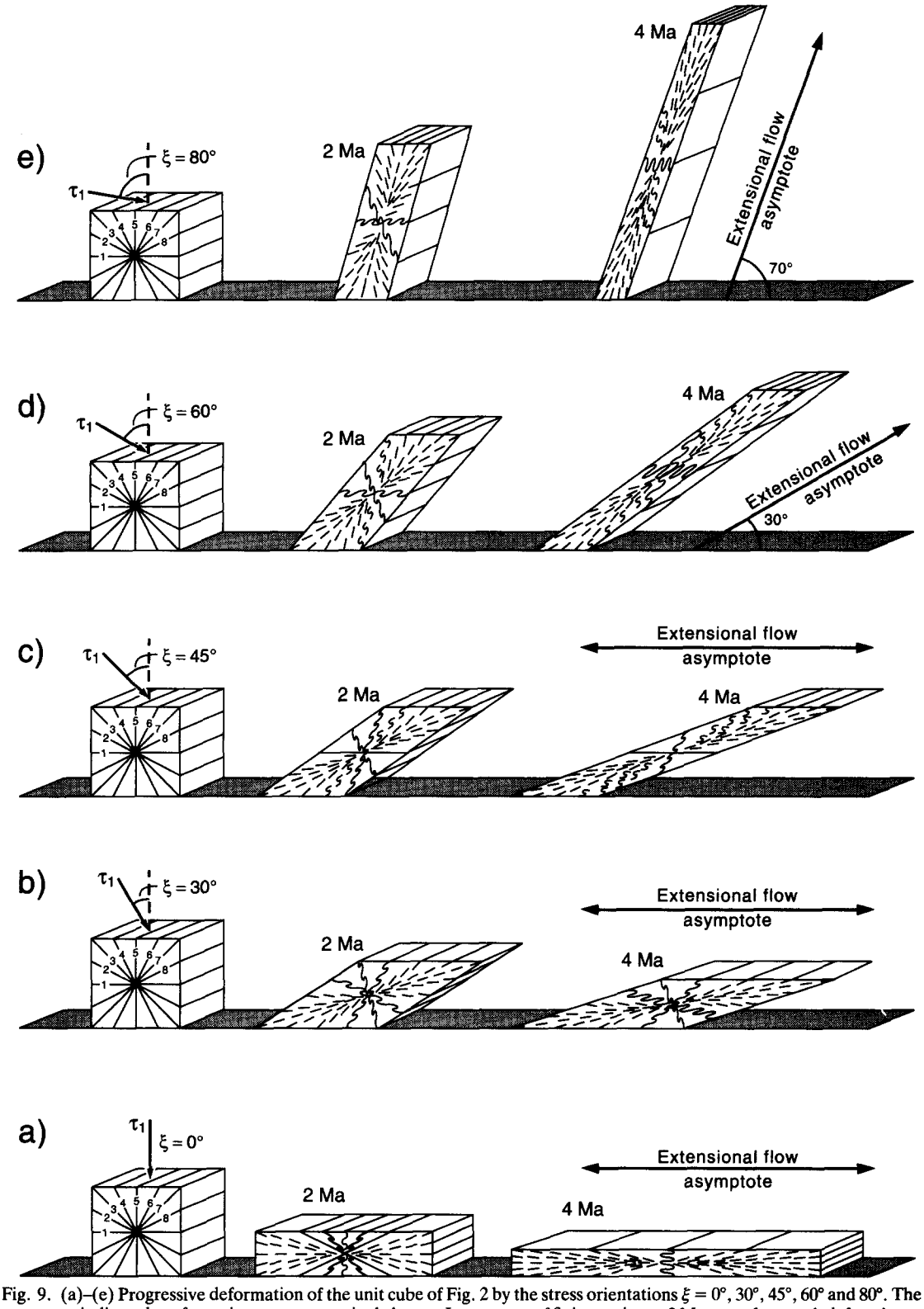

Fig. 9. (a)–(e) Progressive deformation of the unit cube of Fig. 2 by the stress orientations $\xi = 0°, 30°, 45°, 60°$ and $80°$. The structures indicated are for active, competent single layers. Increments of finite strain are 2 Ma apart for a rock deforming at a strain rate of 10^{-14} s^{-1}. The direction of maximum stretch is parallel to the the stretching fault or the X-direction for principal deviatoric stress orientations $0° \leq \xi \leq 45°$. However, the direction of maximum stretch is not parallel to the X-axis but aligned with the orientation of the extensional flow asymptote for deformations where $45° < \xi \leq 90°$. Rotation of material lines towards parallelism with the extensional flow asymptote occurs faster in pure shear deformation than in simple shear deformation (cf. Weijermars 1991).

unique set of two straight streamlines (both solutions of $\psi = 0$), except for $\xi = 45°$, where they coincide. The asymptote to the exit flow, termed here the extensional asymptote, coincides with the X-axis or stretching fault for $0° \leq \xi \leq 45°$. The asymptote to the entrance flow, termed here the compressional asymptote, coincides with the X-axis for $45° \leq \xi \leq 90°$. In the latter case, the direction of the extensional flow asymptote is variable.

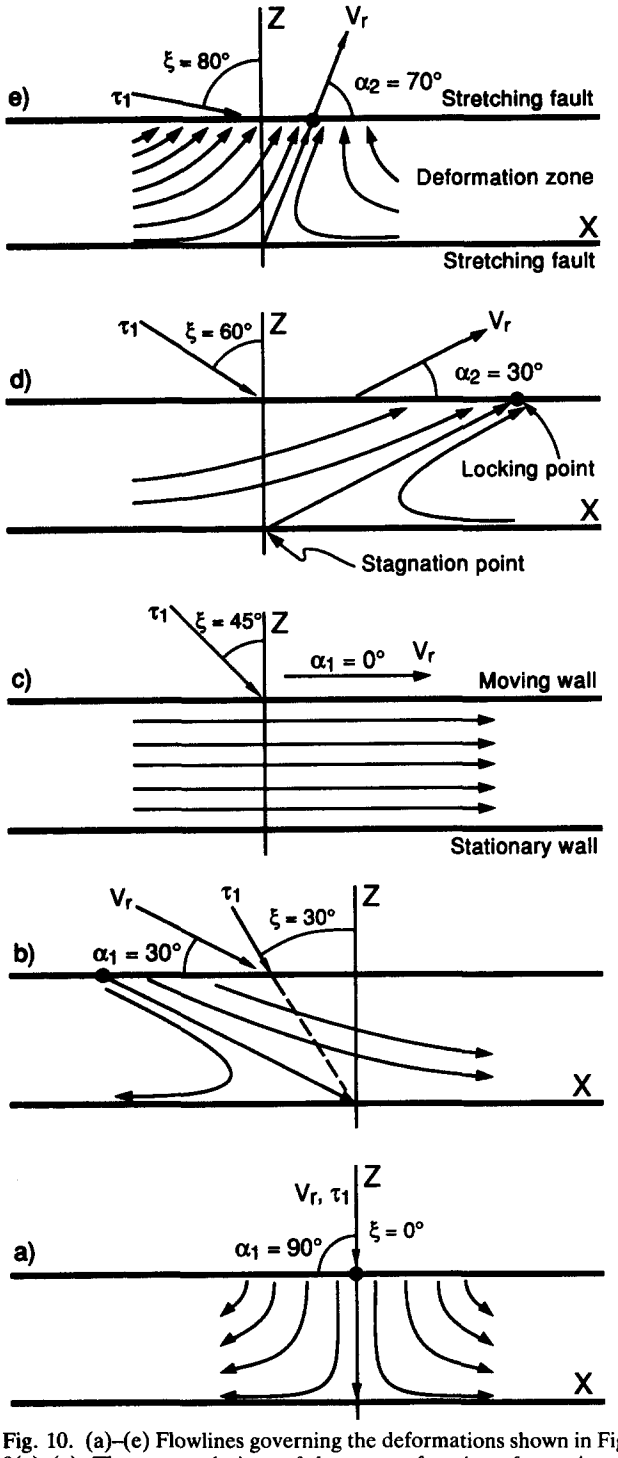

Fig. 10. (a)–(e) Flowlines governing the deformations shown in Figs. 9(a)–(e). These are solutions of the stream function of equation (6) using the stress orientations $\xi = 0°, 30°, 45°, 60°$ and 80°, and arbitrary strain rate $\dot{e}_1$. The inclinations of the flow asymptotes, α_1 and α_2, are governed by equations (7a) and (7b), respectively. The relative velocity vectors, V_r, of the upper boundary of the deforming volume is parallel to the inclined flow asymptotes.

The direction of the compressional flow asymptote, α_1, is given by:

$$\alpha_1 = 90° - 2\xi, \qquad \text{provided } 0° \leq \xi \leq 45°. \quad (7a)$$

The orientation of the extensional flow asymptote, α_2, is given by:

$$\alpha_2 = 2\xi - 90°, \qquad \text{provided } 45° \leq \xi \leq 90°. \quad (7b)$$

Positive angles α_1 are measured clockwise from the X-axis and positive angles α_2 are measured anticlockwise from the X-axis (Fig. 10).

Figure 10 includes information on the relationship between the relative plate motion and the stress orientation within the deformation zone. One principal axis of deviatoric stress coincides with the bisector of the acute angle between the relative velocity vector and the normal to the boundary of the deforming zone, as elaborated elsewhere (Weijermars submitted). The relative velocity vectors, V_r, of the upper boundary of the deforming volume are parallel to the inclined flow asymptotes.

DISCUSSION

It has been common to discuss the length history of material lines by graphically superposing the incremental strain ellipsoid with the finite strain ellipsoid (cf. Ramsay 1967, Ramsay & Huber 1983). Whereas previously the only cases considered were pure and simple shear deformations, the analytical results introduced here allow discussion of any type of homogeneous plane deformation, with special reference to the boundary stresses controlling the deformation. The limiting assumptions made are: (1) homogeneous bulk deformation; (2) no volume change; and (3) plane strain. These three conditions are commonly imposed as boundary conditions in analog experiments using active single layers in pure and simple shear boxes (references cited), and the instabilities observed have been used to confirm predictions based on length changes in passive marker lines. However, potentially tangible effects on the symmetry of folds may occur from amplification of initially asymmetric perturbations (e.g. Abbassi & Mancktelow 1990). Such local complications and deviation from the bulk behaviour are neglected in the present first-order approximation for the sake of generalization. Modelling of active marker layers in advanced analog experiments and numerical simulations may help to improve the generalization attempted here.

The results of the present analysis may be translated into practical rules for constraining bulk palaeostress orientations from the geometry of competent and incompetent single layers or veins. Hints for checking the validity of the assumption underlying the model approach, if applied to field studies, have been discussed elsewhere (Weijermars 1991, 1992). If the limiting conditions hold, the direction of the major principal palaeostress can be constrained as follows.

(1) Determine whether the finite strain is large enough to assume that initially cross-cutting material markers have all become aligned with the extensional flow asymptote. The axes of Figs. 7 and 8 can be scaled with the principal bulk stretch, S_1, instead of the non-dimensional time, R_t, by using $R_t = \ln S_1$. Although this expression is only strictly valid for pure shear deformations, it is still a good approximation even for simple shear for stretches smaller than 3, and provides rough

estimates for larger simple shears (Weijermars 1991). Recall that 4 Ma dimensional time corresponds to a non-dimensional time $R_t = 4 \times 0.315 = 1.26$, which gives a finite stretch $S_1 = 3.5$. This stretch is enough to bring most material lines parallel to the flow asymptotes in pure shear deformations. A stretch of about 10 on a time scale of 8 Ma is required to achieve a similar alignment in simple shear deformations.

(2) Establish whether the flow asymptotes implied by rotated markers are oblique or subparallel to a physical boundary separating the deformed region from adjacent, relatively undeformed rock. If oblique, all parameters are solvable. The compressional flow asymptote is then parallel to the physical boundary and the direction of the extensional flow asymptote is traced by the oblique markers so that $45° \leq \xi \leq 90°$. The actual orientation ξ of the major principal deviatoric stress follows from the angle, α_2, between the two flow asymptotes, by:

$$\xi = (\alpha_2 + 90°)/2. \quad (8)$$

(3) If cross-cutting material line markers have all rotated to become, not oblique, but parallel to the physical boundary, then $0° \leq \xi \leq 45°$. It is assumed that shortening competent layers will fold and extending competent layers boudinage. Likewise, shortening incompetent layers will mullion and extension develops inverse folds which resemble pinch-and-swells if not stretching by uniform thinning. If a competent layer normal to the stretching fault is symmetrically folded then $\xi = 0°$. Layers which have not developed any mechanical instability, neither boudins nor folds, may imply that no change in lengths has occurred and this can only occur in true *simple shear*, $\xi = 45°$. Laboratory experiments have established that lines parallel to the direction of shear in simple shear do not fold unless by attenuation of large initial perturbations (Ramberg 1959, Ghosh 1966). Alternatively, straight parallel layers without any mechanical perturbation could have undergone uniform stretching and it may be difficult in nature to calibrate this against the initial length.

If the preceding tests indicate that $0° \leq \xi \leq 45°$, then the bulk palaeostress orientation may be constrained in terms of the angle, γ, between the stress direction and the enveloping surface of the single layers studied. Figures 11(a)–(f) illustrate the principle for a competent single layer and Figs. 12(a)–(f) show the corresponding cases for an incompetent single layer. Symmetric and non-rotational structures occur only if the bulk deformation is a *pure shear*, so that symmetric folds or symmetric mullions imply that the folded layer was initially parallel to the direction of the major principal stress axis. Similarly, symmetric pinch-and-swells and non-rotated but boudinaged blocks are normal to the direction of the major principal stress axis. Asymmetric folds, asymmetric mullions and rotated boudins and pinch-and-swells all imply that the principal palaeostress axes were oblique to the enveloping surface of the deformed layer. The sense of rotation and asymmetry are not only kinematic indicators, but also constrain the range of possible orientations of the principal stress axes within 0–45° to the enveloping surface of the single layer. Kinematic indicators have to be used in order to be able to decide which of the two possible 45°-directions in *simple shear* is correct. Estimates of the paleostress

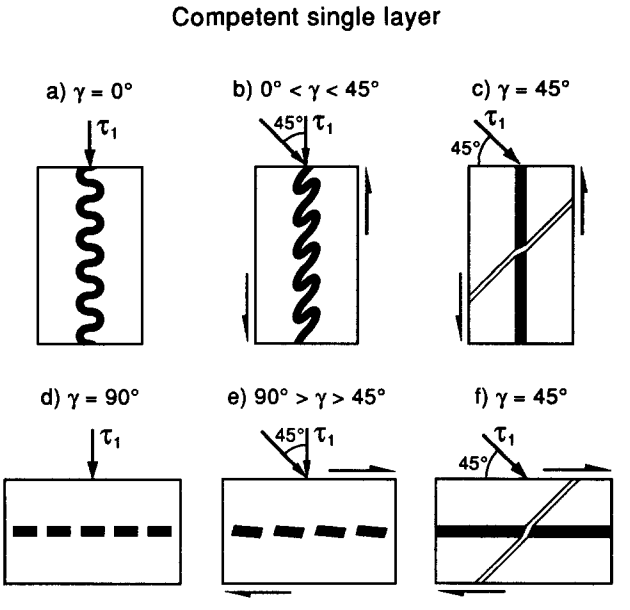

Fig. 11. (a)–(f) Orientations of palaeostress axes may be constrained using the orientation of symmetric and asymmetric structures displayed by *competent* single layers (folds, boudins). The intermediate deviatoric stress, τ_2, is always perpendicular to the plane of view as plane strain is assumed. The direction of strain refraction used as kinematic indicator in (c) is governed by expressions derived by Strömgård (1973), Treagus (1973) and Weijermars (1992). The sense of rotation of the boudins in (e) is in accordance with experiments by Ghosh & Ramberg (1976).

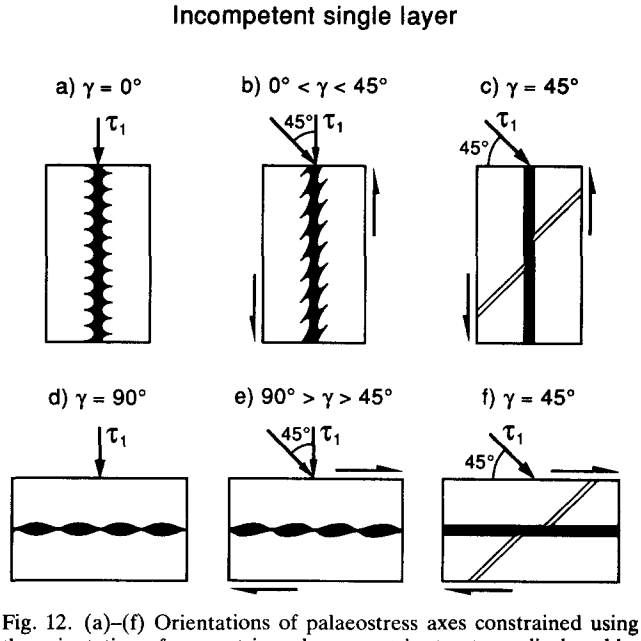

Fig. 12. (a)–(f) Orientations of palaeostress axes constrained using the orientation of symmetric and asymmetric structures displayed by *incompetent* single layers (mullions, inverse folds). The intermediate deviatoric stress, τ_2, is always perpendicular to the plane of view as plane strain is assumed.

directions thus obtained can be calibrated against those determined from the inclination and stretch of the finite ellipse and applying the nomograms of Weijermars (1991).

Obviously, there are also implications for models of the development of a foliation. Assume that the undeformed boxes in Fig. 9 comprise a randomly oriented fabric. The fabric will develop a preferred orientation according to the March passive rotation model and will be enhanced by crystalloplastic flow and recrystallization. The direction of the foliation and associated stretching lineation will rotate towards parallelism with the extensional flow asymptote. This insight can be used to constrain the possible orientations of the major principal deviatoric stress axis, τ_1, with respect to the foliation. In all cases considered here, the angle between the foliation and τ_1 will vary between 45° and 90°. The particular relationship between τ_1, bulk deformation, and boundary movement in anisotropic rocks has been elaborated elsewhere (Weijermars 1992).

Finally, the minimum work paths of progressive deformation as discussed by Nadai (1963) closely correspond to those resulting from a steady stress field. Whether nature is actually bothered by minimum energy requirements is another matter. However, deformations by bulk stresses of steady orientation are inherent to deformation zones confined between two subparallel boundaries converging or diverging without relative rotations (Fig. 10). This insight, together with the knowledge that the tectonic plates which drive deformation have steady directions of relative motion over long periods underlies my assumption that many deformation patterns may have been created in a regionally steady stress field.

Acknowledgements—This work was partly inspired by analog experiments in competent single layers of paraffin wax using modelling facilities developed by Neil Mancktelow at ETH-Zurich. This work has benefitted from helpful discussions and critical comments by Chris Talbot, and review comments by A. J. Watkinson and an anonymous reviewer. The plotting of the graphs of Figs. 7 and 8 was subcontracted to Alexei Poliakov who generated them on a SUN work station using PV-WAVE, a plotting and image display package by Precision Visuals, Inc. Other draftwork was stylized by Jeanette Bergman of Tellurit Datorgrafik. This work has been funded by the Swedish Natural Science Research Council (NFR).

REFERENCES

Abbassi, M. R. & Mancktelow, N. S. 1990. The effect of initial perturbation shape and symmetry on fold development. *J. Struct. Geol.* **12**, 273–282.

Anthony, M. & Wickham, J. 1978. Finite-element simulation of asymmetric folding. *Tectonophysics* **47**, 1–14.

Becker, G. F. 1893. Finite homogeneous strain, flow and rupture in rocks. *Bull. geol. Soc. Am.* **4**, 13–90.

Bergman, J. 1987. Analysis and simulation of a boudinaged quartz vein. Unpublished B.Sc. thesis, University of Uppsala.

Biot, A. M. 1961. Theory of folding of stratified viscoelastic media and its implications in tectonics and orogenesis. *Bull geol. Soc. Am.* **72**, 1595–1620.

Cloos, H. 1947. Boudinage. *Trans. Am. Geophys. Union* **28**, 626–632.

Cobbold, P. R. 1969. An experimental study of the formation of lobe and cusp structures by shortening of an initial sinusoidal contact between two materials of different viscosity. Unpublished B.Sc. thesis, University of London.

Cobbold, P. R., Cosgrove, J. W. & Summers, J. M. 1971. Development of internal structures in deformed anisotropic rocks. *Tectonophysics* **12**, 23–53.

Dieterich, J. M. & Carter, N. L. 1969. Stress history of folding. *Am. J. Sci.* **267**, 129–154.

Emermann, S. E. & Turcotte, D. L. 1984. A back-of-the-envelope approach to boudinage mechanics. *Tectonophysics* **110**, 333–338.

Fletcher, R. C. 1974. Wavelength selection in the folding of a single layer with power-law rheology. *Am. J. Sci.* **274**, 1029–1043.

Fletcher, R. C. 1982. Coupling of diffusional mass transport and deformation in a tight rock. *Tectonophysics* **83**, 275–291.

Flinn, D. 1962. On folding during three dimensional progressive deformation. *Q. J. geol. Soc. Lond.* **118**, 385–433.

Gay, N. C. & Jaeger, J. C. 1975. Cataclastic deformation of geological matrices of differing composition: II. Boudinage. *Tectonophysics* **27**, 323–331.

Ghosh, S. K. 1966. Experimental test of buckling folds in relation to strain ellipsoid in simple shear deformation. *Tectonophysics* **3**, 169–185.

Ghosh, S. K. & Ramberg, H. 1976. Reorientation of inclusions by combination of pure and simple shear. *Tectonophysics* **34**, 1–70.

Hanmer, S. & Passchier, C. 1991. Shear-sense indicators: a review. *Geol. Soc. Can. Pap.* **90-17**.

Hildebrand-Mittlefehldt, N. 1983. Strain fields in and around boudins in a clay experiment. *J. Struct. Geol.* **5**, 465–470.

Hudleston, P. J. 1973. An analysis of "single-layer" folds developed experimentally in viscous media. *Tectonophysics* **16**, 189–214.

Johnson, A. M. 1977. *Styles of Folding*, Elsevier, Amsterdam.

Lloyd, G. E. & Ferguson, C. C. 1981. Boudinage structures: some new interpretations based on elastic-plastic finite element simulations. *J. Struct. Geol.* **3**, 117–128.

Lloyd, G. E., Ferguson, C. C. & Reading, K. 1982. A stress transfer model for the development of extension fracture boudinage. *J. Struct. Geol.* **4**, 355–372.

Means, W. D. 1989. Stretching faults. *Geology* **17**, 893–896.

Means, W. D. 1990. One-dimensional kinematics of stretching faults. *J. Struct. Geol.* **12**, 267–272.

Nadai, A. 1963. *Theory of Flow and Fracture in Solids, Volume* 2. McGraw-Hill, New York.

Neurath, C. & Smith, R. B. 1982. The effect of material properties on growth rates of folding and boudinage: experiments with wax models. *J. Struct. Geol.* **4**: 215–229.

Passchier, C. W. 1986. Flow in natural shear zones—the consequences of spinning flow regimes. *Earth Planet. Sci. Lett.* **77**, 70–80.

Passchier, C. W. 1990a. A Mohr circle construction to plot the stretch history of material lines. *J. Struct. Geol.* **12**, 513–515.

Passchier, C. W. 1990b. Reconstruction of deformation and flow parameters from deformed vein sets. *Tectonophysics* **180**, 185–199.

Passchier, C., Myers, J. S. & Kröner, A. 1990. *Field Geology of High-grade Terrains*. Springer, Berlin.

Paterson, M. S. & Weiss, L. E. 1968. Folding and boudinage of quartz-rich layers in experimentally deformed phyllite. *Bull. geol. Soc. Am.* **79**, 795–812.

Pfiffner, O. A. & Ramsay, J. G. 1982. Constraints on geological strain rates: arguments from finite strain states of naturally deformed rocks. *J. geophys. Res.* **87**, 311–321.

Ramberg, H. 1955. Natural and experimental boudinage and pinch-and-swell structures. *J. Geol.* **63**, 512–526.

Ramberg, H. 1959. Evolution of ptygmatic folding. *Norges geol. Tidsskr.* **39**, 99–152.

Ramberg, H. 1967. *Gravity, Deformation and the Earth's Crust* (1st edn). Academic Press, London.

Ramberg, H. 1975a. Particle paths, displacement and progressive strain applicable to rocks. *Tectonophysics* **28**, 1–37; see also Ramberg's (1986) correction in: *Tectonophysics* **121**, 355.

Ramberg, H. 1975b. Superposition of homogeneous strain and progressive deformation in rocks. *Bull. Geol. Inst. Univ. Uppsala, N.S.* **6**, 35–67.

Ramberg, H. 1981. *Gravity, Deformation and the Earth's Crust* (2nd edn). Academic Press, London, 452 pp.

Ramsay, J. G. 1967. *Folding and Fracturing of Rocks*. McGraw-Hill, New York, 1–568.

Ramsay, J. G. & Huber, M. H. 1983. *The Techniques of Modern Structural Geology, Volume* 1: *Strain Analysis*. Academic Press, London.

Roberts, D. & Strömgård, K.-E. 1972. A comparison of natural and experimental strain patterns around fold hinge zones. *Tectonophysics* **14**, 105–120.

Selkman, S. 1978. Stress and displacement analysis of boudinage by the finite-element method. *Tectonophysics* **44**, 115–139.

Shimamoto, T. & Hara, I. 1976. Geometry and strain distribution of single-layer folds. *Tectonophysics* **30**, 1–34.

Smith, R. B. 1975. Unified theory of the onset of folding and mullion structure. *Bull. geol. Soc. Am.* **86**, 1601–1609.

Smith, R. B. 1977. Formation of folds, boudinage, and mullions in non-Newtonian materials. *Bull. geol. Soc. Am.* **88**, 312–320.

Smith, R. B. 1979. The folding of a strongly non-Newtonian layer. *Am J. Sci.* **279**, 272–287.

Sokoutis, D. 1987. Finite strain effects in experimental mullions. *J. Struct. Geol.* **9**, 233–242.

Soloutis, D. 1990. Experimental mullions at single and double interfaces. *J. Struct. Geol.* **12**, 365–373.

Strömgård, K.-E. 1973. Stress distribution during formation of boudinage and pressure shadows. *Tectonophysics* **16**, 215–248.

Talbot, C. J. 1970. The minimum strain ellipsoid using deformed quartz veins. *Tectonophysics* **9**, 47–76.

Talbot, C. J. & Sokoutis, D. 1992. The importance of incompetence. *Geology* **20**, 951–953.

Treagus, S. H. 1973. Buckling stability of a viscous single-layer system, oblique to the principal compression. *Tectonophysics* **19**: 271–289.

Troëng, B. 1975. One natural and some experimental pinch-and-swell structures. *Geol. För. Stock. Förh.* **97**, 383–386.

Weijermars, R. 1991. The role of stress in ductile deformation. *J. Struct. Geol.* **13**, 1061–1078.

Weijermars, R. 1992. Progressive deformation in anisotropic rocks. *J. Struct. Geol.* **14**, 723–742.

Weijermars, R. & Poliakov, A. In press. Stream functions and complex potentials: Implications for development of rock fabric and the continuum assumption. *Tectonophysics* **220**.